The Local Flow around the Upstream Side of Bridge Piers

AUTHOR(S):

UTAMI, Tadashi

CITATION:

UTAMI, Tadashi. The Local Flow around the Upstream Side of Bridge Piers. Bulletin of the Disaster Prevention Research Institute 1975, 25(4): 55-75

ISSUE DATE:

1975-12

URL:

http://hdl.handle.net/2433/124853

The Local Flow around the Upstream Side of Bridge Piers

By Tadashi UTAMI

(Manuscript received December 19, 1975)

Abstract

The local flow around bridge piers has such a complicated mechanism due to fluctuations and three-dimensionality that the result of analytical study has not explained clearly the horseshoe vortex and down flow which characterize this local flow and play an important role on local scour.

In this paper the author attempts first to make clear the fundamental characteristics of the local flow by experiments. For that purpose detailed measurements are made under laminar conditions as well as under turbulent conditions on the flow around a pier settled on the flat bed of a channel. He attempts secondly to propose a flow model on the basis of the experimental results in order to analyse the three-dimensional characteristics of local flows. Lastly, the results of the analysis are shown to be in fairly good agreement with the measured value.

1. Introduction

It is said[1)-7)] that the local scour around a bridge pier is due to horseshoe vortices which occur just at the upstream side of the pier. The analytical studies of these local flows are considered to be divided into two categories: One is the analyses by Ogawa et al[8)] and Kikkawa et al[9)], in which the down flow in front of the pier is explained as the result of the vertical difference of pressure due to velocity distribution of an approaching flow, and the other is the analyses by Shen et al[7)] and Nakagawa et al[10)], in which the formation of the horseshoe vortex is attempted to be explained as the deformation process of vorticity, which had been contained in the approaching flow. However, because of three-dimensionality and fluctuation, the structure of a horseshoe vortex is so complicated that neither analysis is sufficient to clearly explain about the process by which the vortex occurs.

Accordingly, it is considered important first to make clear the fundamental characteristics of the vortex motion by means of a detailed measurement in the experiments conducted under such simplified conditions as possible, and second to construct a flow model applicable to formulate the flow around bridge piers on the basis of the experimental results.

2. Experimental Study of the Local Flow under Laminar Conditions

(1) Method of Experiments

The horseshoe vortex is said to occur as the result of the concentration of vortices which had been contained in the main flow. It is reasonable to consider

that this is a common characteristic to either laminar or turbulent conditions. So, the results of experiments conducted under laminar conditions, in which visual measuring methods, e. g. hydrogen bubble method, are used more successfully, will be useful to guess the characteristics of time averaged flow under turbulent conditions, which is complicated.

The experimental channel, which is made of lucid acrylic plates in order to make possible the visual observations, is uniform, 20cm wide and 6m long with a bed slope of 1/500.

Laminar flow conditions were attained by making use of water mixed with glycerine. As kinematic viscocity of the liquid is about 5.6 cm^2/sec, experiments were made at as low Reynolds number as 2.0～3.0. The velocity distribution of approaching flow is recognized as being nearly parabolic in the central section of the channel. Experimental conditions are shown in Table 1.

Table 1 Experimental conditions (in case of laminar flow)

run	water depth H (cm)	suface velocity U_{0s} (cm/sec)	ν (cm/sec)	pier diameter $2r_0$ (cm)	$\frac{HU_{0s}}{\nu}$	$\frac{2r_0U_{0s}}{\nu}$	cross-section of pier
A-3	4.63	3.74	5.62	5.00 (side length)	3.08	3.33	square
D-4	3.92	2.66	5.67	4.025	1.84	1.89	circle
D-5	〃	〃	〃	5.00	〃	2.35	〃

(2) Results of Experiments

As mentioned above, the hydrogen bubble method was successfully used in laminar flow and examples of results of measurement by this method are shown in Photo. 1.

Fig. 1 shows the pattern of stream lines measured by the hydrogen bubble method in the stagnation plane upstream of the pier with square crosssection, and Fig. 2 shows

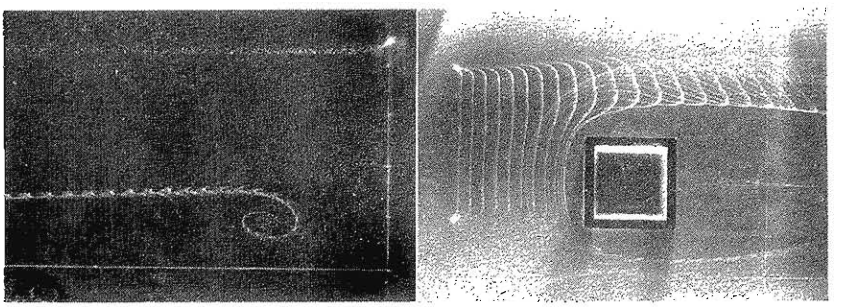

(a) flow pattern in the stagnation plane (b) flow pattern riewed from below.

Photo. 1 Visualized flow pattern by hydrogen bubble method

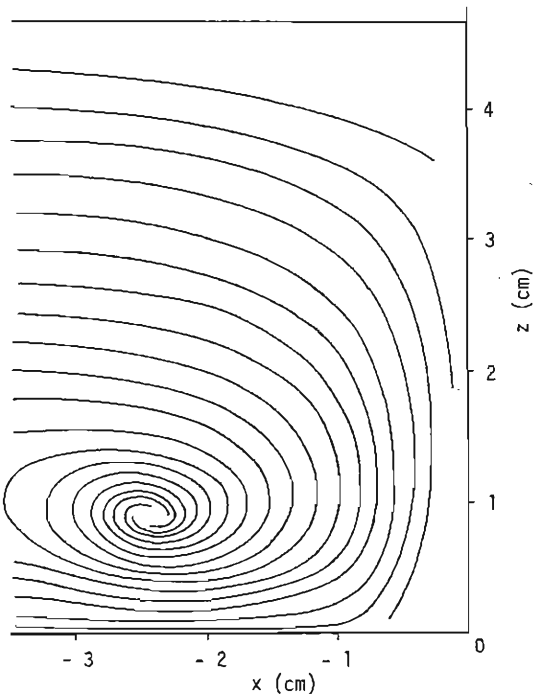

Fig. 1 Pattern of streamlines in the stagnation plane upstream of a pier with a square crosssection (run A-3)

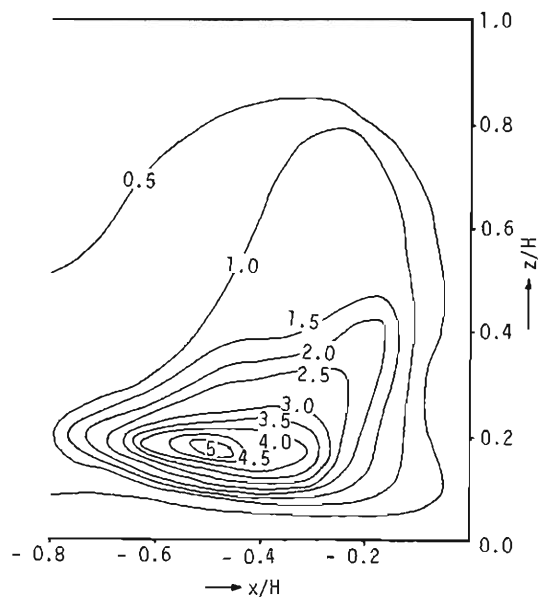

Fig. 2 Distribution of vorticity η calculated from the measured distribution of velocity in the stagnation plane (run A-3)

the distribution of vorticity η calculated from the measured distribution of velocity. It becomes clear from these that the liquid composing the horseshoe vortex is supplied from a part of the main flow and vorticity is concentrated in the neighbourhood of the vortex axis.

Let us consider a vortex tube which has unit crosssectional area at a point sufficiently upstream of the pier. As it flows down, the crosssectional area becomes α, and the distribution of $\alpha\eta$ in the stagnation plane is calculated from experimental results as shown in Fig. 3. Comparing Fig. 3 with Fig. 1, it is recognized that the value of $\alpha\eta$ is nearly constant along each stream line, from which it becomes clear that the Helmholtz's conservation law of vorticity holds for the concentration of vorticity.

In the experiments of the flow around piers with circular crosssection, the concentration of vorticity is also recognized. In these experiments it also becomes clear that the axis of horseshoe vortex is nearly concentric with the pier and is parallel to the channel bed.

3. Analytical Study of the Local Flow under Laminar Conditions

(1) Formation of Flow Model

Let us consider the flow around a circular pier of radius r_0. Supposing the flow is composed of main flow and secondary flow [1),12),13)] and the main flow is irrotational in the section parallel to the channel bed, r, θ and z components of velocity of main flow may be written

$$u_r = U_0\{1-(r_0/r)^2\}\cos\theta \qquad (1)$$

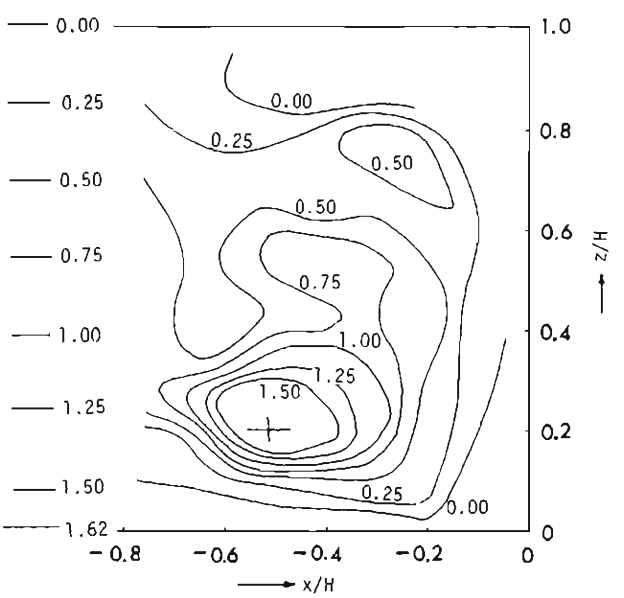

Fig. 3 Distribution of $\alpha\eta$ in the stagnation plane calculated from experimental results (run A-3)

$$u_\theta = -U_0\{1+(r_0/r)^2\}\sin\theta \tag{2}$$

$$u_z = 0 \tag{3}$$

where U_0 is the velocity distribution of approaching flow and is written for the case of laminar flow

$$U_0/U_{0s} = (z/H)(2-z/H) \tag{4}$$

$$U_{0s} = gH^2 i/2\nu \tag{5}$$

As for the secondary flow, on the basis of the experimental results that the vorticity is concentrated in the neighbourhood of the vortex axis, we may compose the flow model, in which vorticity $\omega=\omega(\theta)$ that gives rise to secondary flow is supposed to exist only in the doughnut type region as shown in Fig. 4. Based on this flow model, the stream function ψ of the secondary flow may be written

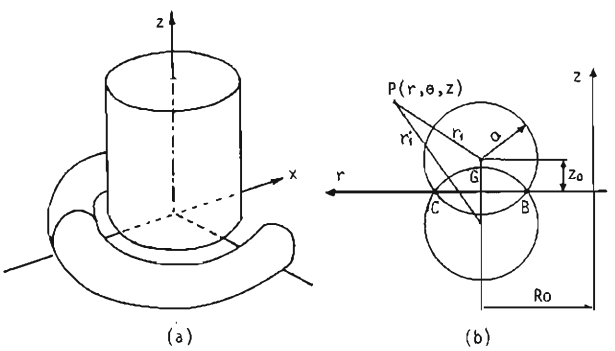

Fig. 4 The vortex region which gives rise to the secondary flow in the flow model

$$\psi = \psi_1 + \psi_2 \tag{6}$$

where, inside the vorticity region[14],

$$\psi_1 = -(\kappa/2\pi)R_0\{\log(8R_0/a) - 3/2 - (r_1/a)^2/2\} \tag{7}$$

and outside the vorticity region[14],

$$\psi_1 = -(\kappa/2\pi)R_0\{\log(8R_0/r_1) - 2\} \tag{8}$$

and ψ_2 is the image of ψ_1 against the channel bed, and $\kappa=\pi a^2\omega$.

The three-dimensional velocity distribution is supposed to be given by adding the velocity component of secondary flow to that of the main flow. On the other hand, on the experimental result that the vortex axis is stationary, the r component of velocity must be zero along the vortex axis. From which κ is written

$$\kappa = \frac{\pi\delta^2 U_{0s}}{H}\left(2-\frac{z_0}{H}\right)\left(1-\frac{r_0^2}{R_0^2}\right)\cos\theta \tag{9}$$

where, $\delta = \{|a-2z_0| + (a+2z_0)\}/2$ (10)

Thus the three-dimensional velocity distribution is written as follows.

1. In the region $r_1 \leqq a$ and $r_1' \leqq a$

$$\frac{U_r}{U_{0s}} = -\frac{R_0\delta^2}{a^2 r}\frac{z_0}{H}\left(2-\frac{z_0}{H}\right)\left(1-\frac{r_0^2}{R_0^2}\right)\cos\theta + \frac{z}{H}\left(2-\frac{z}{H}\right)\left(1-\frac{r_0^2}{r^2}\right)\cos\theta \tag{11}$$

$$\frac{U_\theta}{U_{0s}} = -\frac{z}{H}\left(2-\frac{z}{H}\right)\left(1+\frac{r_0^2}{r^2}\right)\sin\theta \tag{12}$$

$$U_z = 0 \tag{13}$$

2. In the region $r_1 \leqq a$ and $r_1' > a$

$$\frac{U_r}{U_{0s}} = -\frac{R_0\delta^2}{2H}\left(2-\frac{z_0}{H}\right)\left(1-\frac{r_0^2}{R_0^2}\right)\frac{1}{r}\left(-\frac{z-z_0}{a^2}+\frac{z+z_0}{r_1'^2}\right)\cos\theta + \frac{z}{H}\left(2-\frac{r}{H}\right)\left(1-\frac{r_0^2}{r^2}\right)\cos\theta \tag{14}$$

$$\frac{U_\theta}{U_{0s}} = -\frac{z}{H}\left(2-\frac{r}{H}\right)\left(1+\frac{r_0^2}{r^2}\right)\sin\theta \tag{15}$$

$$\frac{U_z}{U_{0s}} = \frac{R_0\delta^2}{2H}\left(2-\frac{z_0}{H}\right)\left(1-\frac{r_0^2}{R_0^2}\right)\frac{r-R_0}{r}\left(-\frac{1}{a^2}+\frac{1}{r_1'^2}\right)\cos\theta \tag{16}$$

3. In the region $r_1 > a$ and $r_1' > a$

$$\frac{U_r}{U_{0s}} = -\frac{R_0\delta^2}{2H}\left(2-\frac{z_0}{H}\right)\left(1-\frac{r_0^2}{R_0^2}\right)\frac{1}{r}\left(-\frac{z-z_0}{r_1^2}+\frac{z+z_0}{r_1'^2}\right)\cos\theta + \frac{z}{H}\left(2-\frac{z}{H}\right)\left(1-\frac{r_0^2}{r^2}\right)\cos\theta \tag{17}$$

$$\frac{U_\theta}{U_{0s}} = -\frac{z}{H}\left(2-\frac{z}{H}\right)\left(1+\frac{r_0^2}{r^2}\right)\sin\theta \tag{18}$$

$$\frac{U_z}{U_{0s}} = \frac{R_0\delta^2}{2H}\left(2-\frac{z_0}{H}\right)\left(1-\frac{r_0^2}{R_0^2}\right)\frac{r-R_0}{r}\left(-\frac{1}{r_1^2}+\frac{1}{r_1'^2}\right)\cos\theta \tag{19}$$

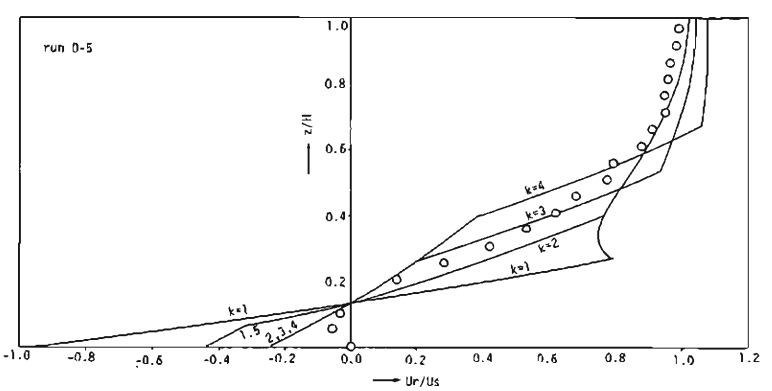

Fig. 5 Experimental verification of equations (11), (14) and (17) with regard to the velocity distribution on the vertical line passing the vortex axis in the stagnation plane (run D-5)

Applying the above equations, the velocity distribution is calculated along the line which is vertical to the channel bed and passes the vortex axis in the stagnation plane. The result is shown in Fig. 5, from which it is recognized that the calculated values show the best agreement with measured values when $k=2$ where k denotes the ratio a/z, so that k shall be equal to 2 in the calculation of velocity.

(2) Verification by Experiments

The above mentioned analysis contains some assumptions and approximations. Especially the approximation that the flow is given by adding secondary flow to main flow does not suffice the dynamical exactitude. Accordingly, the results of analysis may have some restrictions to be applied. So, the applicability of the analysis shall be examined by comparing results of calculation to that of experiments.

In Fig. 6 the distribution of the z component of velocity in stagnation plane is shown, where curved lines show the calculated value of equations (11) $\sim$ (19) and spots show the results of experiments. It can be seen from the figure that the calculated

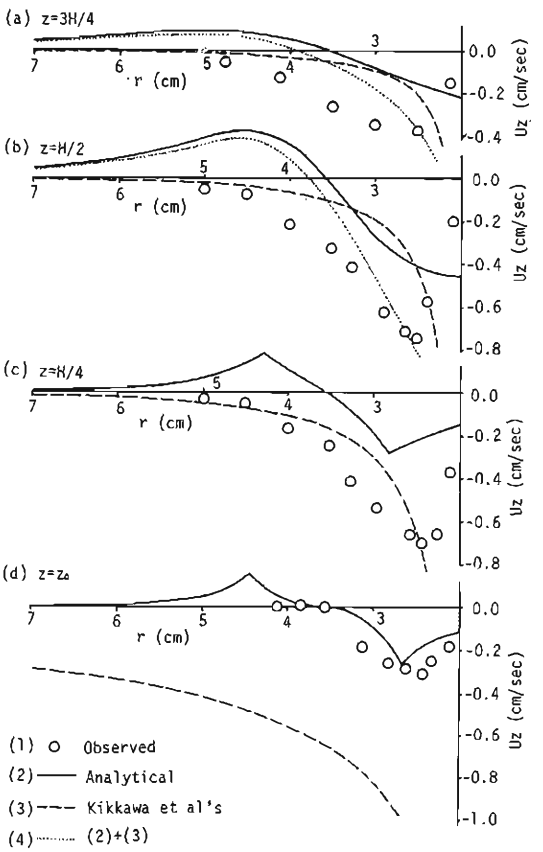

Fig. 6 Experimental verification of equations (11) $\sim$ (19) with regard to the z component of velocity in the stagnation plane (run D-4)

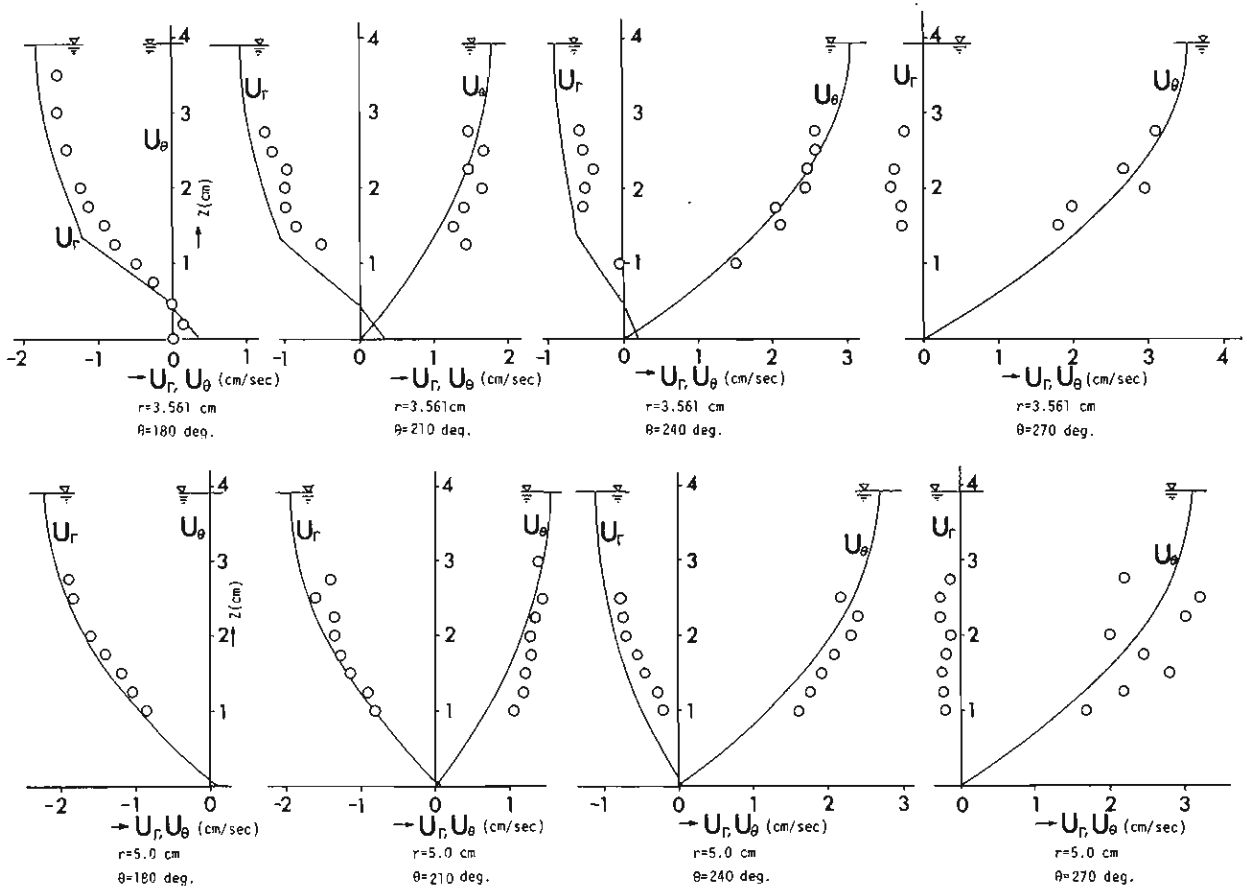

Fig. 7 Experimental verification of equations (11) ~ (19) with regard to r and θ components of velocity (run D-5)

values show fairly good agreement with the measured value, especially in the neighbourhood of the vortex. On the other hand, the calculated results of the equation given by Kikkawa et al[9] show fairly good agreement in the neighbourhood of the water surface, which may be because the author's model is composed on the basis of experimental results that vorticity is concentrated in the neighbourhood of the vortex, while Kikkawa et al examined the velocity distribution in the region outside the vortex.

In Fig. 7 vertical distribution of U_r and U_θ at $r=3.561$ cm (position of vortex axis) and $r=5.0$ cm in each section of $\theta=180°$, 210°, 240° and 270° are shown. The agreement between calculated values and measured ones is recognized to be fairly good.

4. Experimental Study of the Local Flow under Turbulent Conditions

Horseshoe vortices have also been observed around a pier in turbulent conditions as shown in the stereographs of Photo. 2, which were taken with two cameras by using liquid particles as tracer. As these vortices fluctuate with time, the three-dimensional characteristics of time averaged flows, which is considered important in researching local scour around bridge piers in turbulent conditions, is investigated in section 4

Table 2 Experimental conditions (in case of turbulent flow)

run	water depth H (cm)	discharge Q (l/s)	mean velocity U_{0m} (cm/s)	width B (cm)	channel slope i	Fr	pier diameter $2r_0$ (cm)	$\frac{H \cdot U_{0m}}{\nu}$
K - 1	7.40	9.62	32.50	40.0	1/500	0.382	8.0	24,050
L	12.05	5.90	12.20	〃	1/1.000	0.111	10.0	14,701
G 1- 0	1.20	0.77	32.68	〃	〃	0.468	1.5～10.5	1,925
10- 0	5.19	9.43	45.04	〃	〃	0.632	〃	23,550
10-15	7.48	〃	31.48	〃	〃	0.368	〃	〃
10- 3	12.10	〃	19.48	〃	〃	0.179	〃	〃
10- 8	5.74	〃	41.03	〃	〃	0.547	〃	〃
20- 0	8.10	20.00	61.73	〃	〃	0.693	〃	50,000
20- 3	10.17	〃	49.16	〃	〃	0.492	〃	〃
20- 8	15.50	〃	32.26	〃	〃	0.262	〃	〃
20-14	21.52	〃	23.23	〃	〃	0.160	〃	〃
30- 0	10.34	30.00	72.53	〃	〃	0.721	〃	75,000
30- 3	12.05	〃	62.24	〃	〃	0.573	〃	〃
30- 8	17.95	〃	41.78	〃	〃	0.315	〃	〃
40- 0	12.88	40.00	77.64	〃	〃	0.691	〃	100,000
40- 3	13.93	〃	71.79	〃	〃	0.614	〃	〃
40- 8	19.95	〃	50.13	〃	〃	0.359	〃	〃

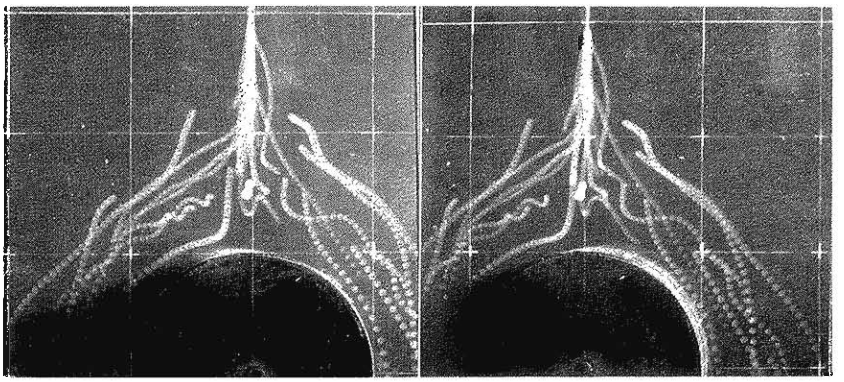

Photo. 2 Visualized flow pattern by liquid particles (run L)

and 5. Conditions of the run of experiments are shown in Table 2.

(1) Three-dimensional Flow Patterns

Fine sands scattered upstream of the pier are arranged on the channel bed by flow, an example of which is shown in Fig. 8 which was obtained under experimental conditions of run L. In this figure a concentric pattern of sand is seen, which was arranged by the reverse flow due to horseshoe vortex.

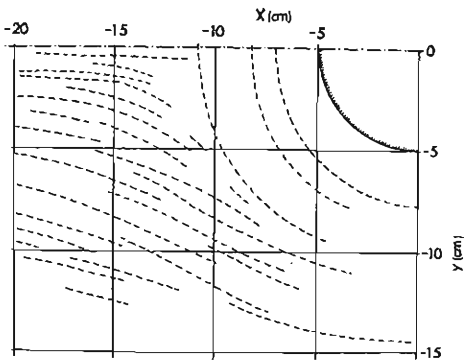

Fig. 8 Pattern of fine sand scattered upstream of the pier (run L)

On the other hand, the time averaged pattern of stream lines in the stagnation plane is observed by using milk as a tracer and is shown schematically in Fig. 9. As shown in both figures, some vortex motions are observed around a bridge pier in case of turbulent conditions. Though both of them fluctuate with time, the vortex A_1 that is nearest to the pier has the largest scale and is most stable, and shall be called the main vortex hereafter. In comparison with the main vortex, the other vortices have smaller scales and are more unstable, and those shall be called small vortices.

(2) Sources of Fluid Constituting the Vortices

In Fig. 9, it is also observed that the fluid constituting these vortices is supplied

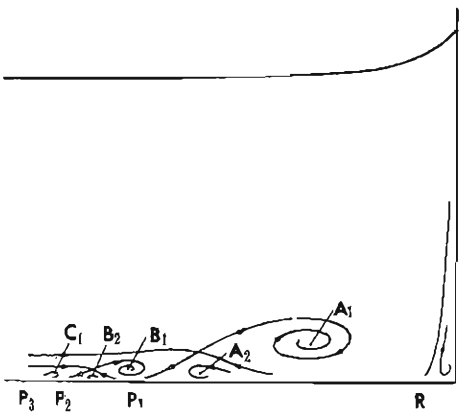

Fig. 9 Schematic pattern of time averaged streamlines in the stagnation plane under tubulent conditions

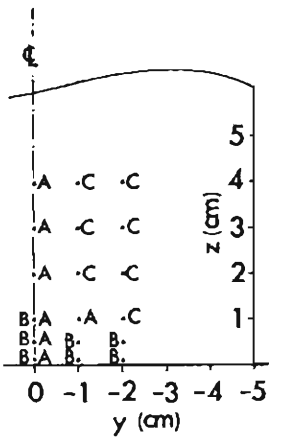

Fig. 10 The region to which the fluid passing through each point in transversal section $x=-10$cm is usually introduced
A ; to main vortex region
B ; to small vortices region
C ; to main flow region

from the main flow, which has similar characteristics to ones observed under laminar conditions. From this fact, it is reasonable to consider that under turbulent conditions the horseshoe vortices also occur due to concentration of vorticity, which had been contained in the main flow.

Fig. 10 shows from which part of the main flow the fluid constituting these vortices are supplied. That is, the fluid passing the point denoted by A in $x=-10$cm plane is usually introduced into the main vortex region, the fluid passing the point denoted by B, into small vortices, and the fluid passing the point denoted by C, into the main flow. It is recognized that the part of the main flow which is introduced into the main vortex region passes through a restricted area near the center line in

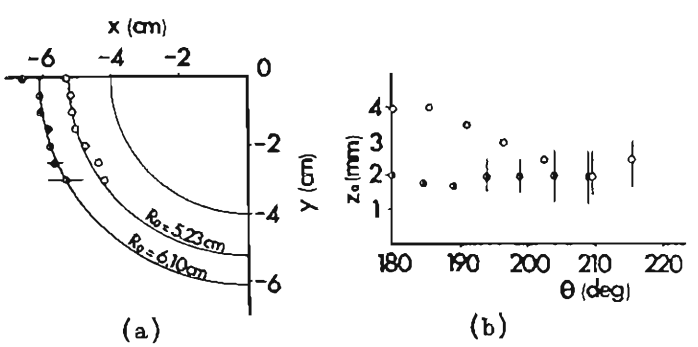

Fig. 11 Time averaged positions of axes of the main vortex and the largest of small vortices (run K-1)

transversal sections in the upstream side of the pier, and the transversal width of the area is at most 1/5 of the diameter of the pier.

(3) Position of Vortex Axis

Time averaged positions of axes of a main vortex and the largest of small vortices were measured by using milk as a tracer and the results are shown in Fig. 11, where R_0 means the distance between the vortex axis and the pier axis, and z_0 means the height of vortex axis from the channel bed. It is recognized that the axis of the main vortex is nearly concentric with the pier and parallel to the channel bed.

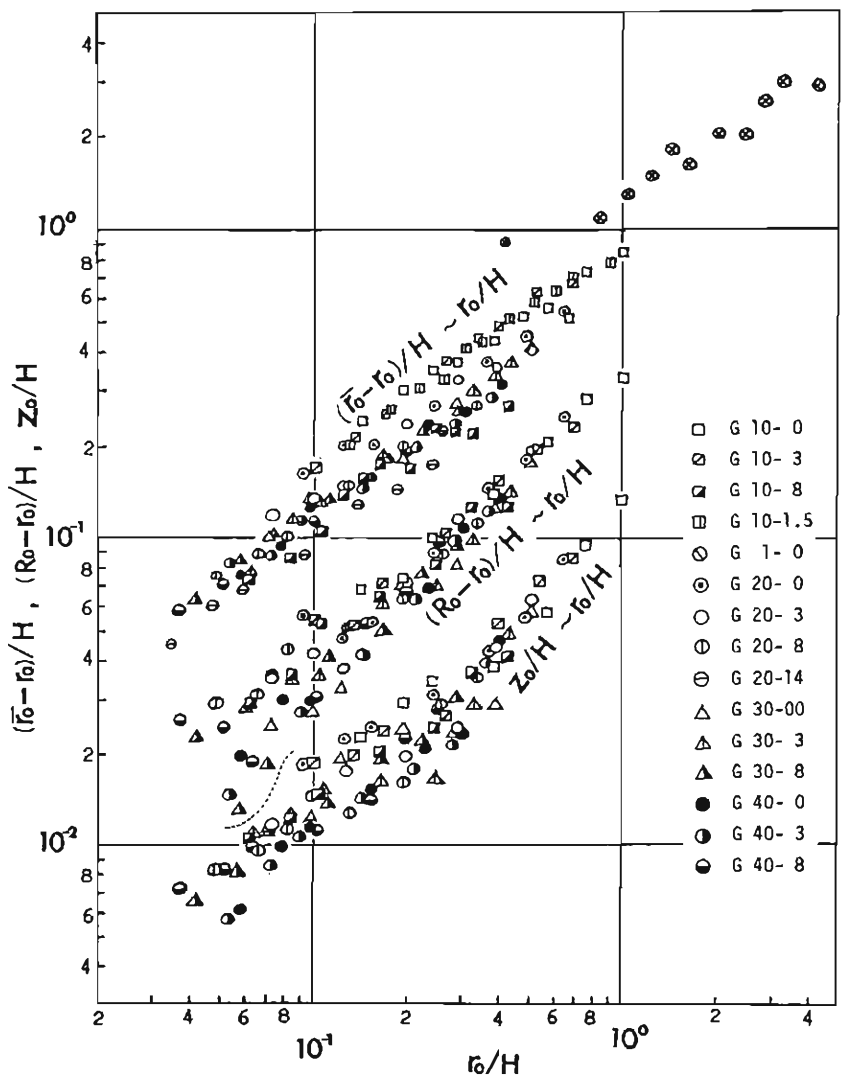

Fig. 12 Time averaged positions of axes of main vortices and radii of displacement areas in stagnation planes

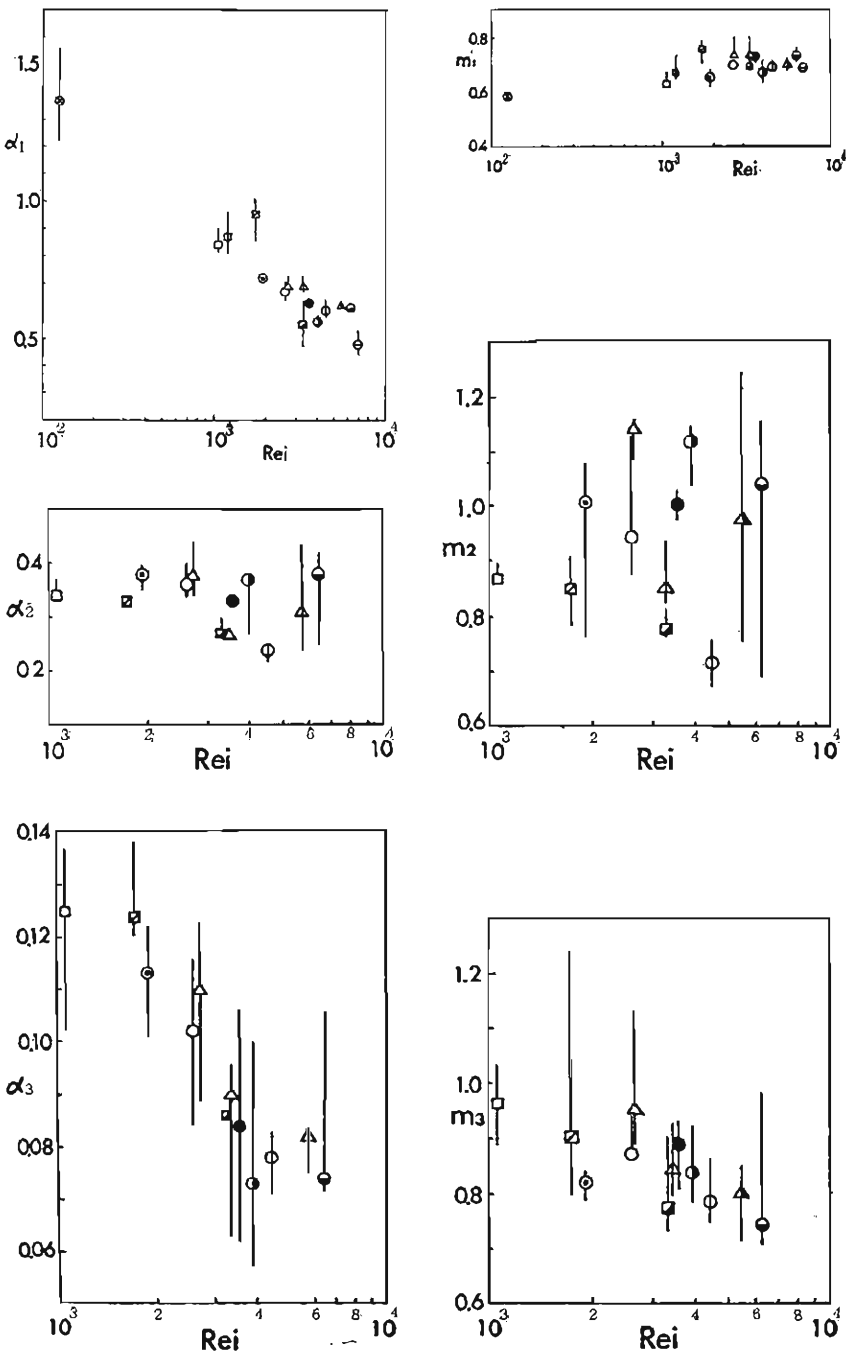

Fig. 13 Relation of each of coefficients $\alpha_1 \sim \alpha_3$ and $m_1 \sim m_3$ to Reynolds number calculated by using water depth and friction velocity

The positions of main vortex axes (R_0, z_0) in the stagnation plane and the radius $\bar{r}_0$ of the displacement area, which is defined by the outermost concentric circle and shows the scale of vortex region, were measured under various experimental conditions and the results are shown in Fig. 12. From this figure it is recognized that each of $(\bar{r}_0-r_0)/H$, $(R_0-r_0)/H$ and z_0/H varies as an exponential function of r_0/H under the condition of constant Q and H. Accordingly, the following representations are attained

$$(\bar{r}_0-r_0)/H=\alpha_1(r_0/H)^{m1} \tag{20}$$

$$(R_0-r_0)/H=\alpha_2(r_0/H)^{m2} \tag{21}$$

$$z_0/H=\alpha_3(r_0/H)^{m3} \tag{22}$$

where $\alpha_1\sim\alpha_3$ and $m_1\sim m_3$ are coefficients determined by the hydraulic conditions of approaching flow. The relation of each of these coefficients to Reynolds number R_{ei} (calculated by using water depth and friction velocity) is shown in Fig. 13.

(4) Velocity Distribution Measured by Hot-Film Velocity Meter

Distributions of time averaged velocity measured by hot-film velocity meter under the flow condition of run K-1 are shown in Fig. 14 together with the time averaged

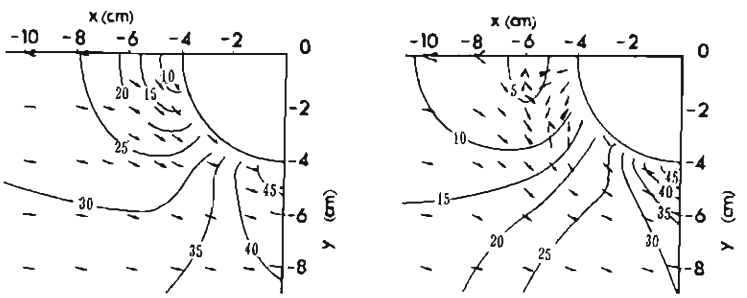

(a) section $z=6$cm (b) section $z=0.2$cm

Fig. 14 Distributions of time averaged velocities measured by hot-film flow meter (run K-1)

flow direction measured by injected dye. The existance of reverse flow at the upstream side of the pier in the section $z=0.2$ cm means that the flow pattern of this section is different from one of irrotational flow. However, as shown in Fig. 15, the distribution of θ component of measured velocity in the section $z=0.2$ cm agrees fairly well with the calculated value of irrotational flow. This fact means that the flow model that the flow is supposed to be consist of an irrotational main flow and a rotational secondary flow is also applicable to a flow under turbulent conditions, because θ component of a secondary flow in this flow model becomes zero when a vortex axis is concentric with the pier.

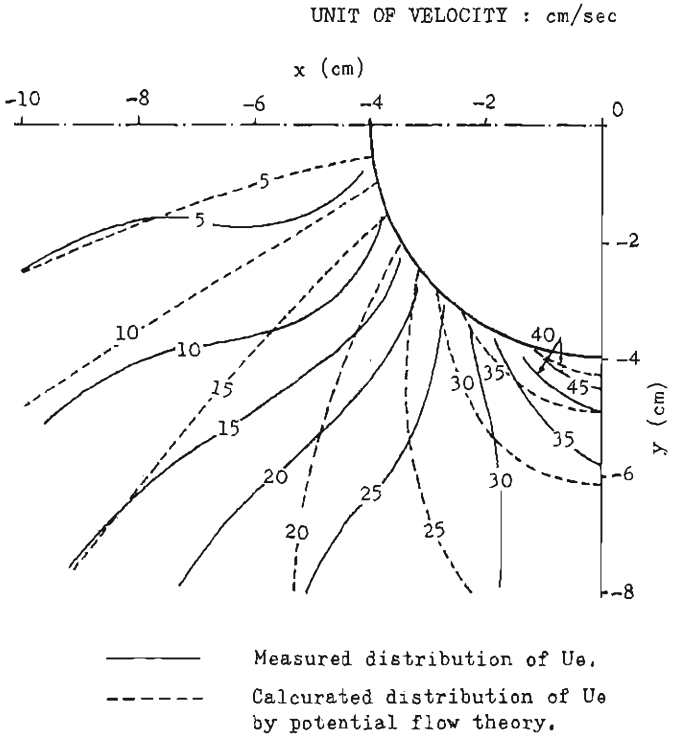

Fig. 15 Comparison between measured velocity in the section $z=0.2$cm and the calculated velocity by irrotational flow theory (run K-1)

5. Analytical Study of the Local Flow under Turbulent Conditions

(1) Applicability of the Flow Model to Turbulent Flow

It became clear that the local flow characteristics under turbulent conditions have an important analogy with those under laminar conditions. Especially, the occurrence of horseshoe vortices due to concentration of vorticity is an important common phenomenon under either condition. However, at the same time, there is also some difference between these two conditions, such as existence of turbulent fluctuations, distribution of approaching velocity, and the number and position of horseshoe vortices.

In this paper, three-dimensional distribution of time averaged velocity will be investigated. Accordingly, as the first approximation, the effects of turbulent fluctuations and small vortices are neglected. On the basis of these approximations and the experimental result that the flow can reasonably be considered to consist of irrotational main flow and rotational secondary flow, the flow model mentioned in 2 is also applicable for the flow in turbulent conditions by a little modification.

(2) Three-Dimensional Distribution of Mean Velocity

Let us consider the turbulent flow around a circular pier of radius r_0. On the

basis of the above consideration, the flow is supposed to be composed of a main flow and a secondary flow.

The main flow may also be given by equations (1)～(3), where, velocity distribution of approaching flow U_0 is written

$$U_0/U_{0s}=(z/H)^{+} \tag{23}$$

As for the secondary flow, the same representations are attained as equations (6) ～ (8), because the vortex motion that gives rise to the secondary flow is approximately supposed to be the main vortex.

Because distributions of time averaged velocities are of concern in this paper, r component of velocity along vortex axis may be considered zero by neglecting turbulent fluctuations. From which κ is written as follows

$$\kappa=\frac{\pi\delta^2 U_{0s}}{z_0}\left(\frac{z}{H}\right)^{+}\left(1-\frac{r_0^2}{R_0^2}\right)\cos\theta \tag{24}$$

where, δ is given by equation (10).

Thus the three-dimensional velocity distribution under turbulent conditions is written as follows

1. In the region $r_1\leqq a$ and $r_1'\leqq a$

$$\frac{U_r}{U_{0s}}=-\frac{R_0\delta^2}{a^2 r}\left(\frac{z_0}{H}\right)^{+}\left(1-\frac{r_0^2}{R_0^2}\right)\cos\theta+\left(\frac{z}{H}\right)^{+}\left(1-\frac{r_0^2}{r^2}\right)\cos\theta \tag{25}$$

$$\frac{U_\theta}{U_{0s}}=-\left(\frac{z}{H}\right)^{+}\left(1+\frac{r_0^2}{r^2}\right)\sin\theta \tag{26}$$

$$U_z=0 \tag{27}$$

2. In the region $r_1\leqq a$ and $r_1'>a$

$$\frac{U_r}{U_{0s}}=-\frac{R_0\delta^2}{2z_0}\left(\frac{z_0}{H}\right)^{+}\left(1-\frac{r_0^2}{R_0^2}\right)\frac{1}{r}\left(-\frac{z-z_0}{a^2}+\frac{z+z_0}{r_1'^2}\right)\cos\theta$$
$$+\left(\frac{z}{H}\right)^{+}\left(1-\frac{r_0^2}{r^2}\right)\cos\theta \tag{28}$$

$$\frac{U_\theta}{U_{0s}}=-\left(\frac{z}{H}\right)^{+}\left(1+\frac{r_0^2}{r^2}\right)\sin\theta \tag{29}$$

$$\frac{U_z}{U_{0s}}=\frac{R_0\delta^2}{2z_0}\left(\frac{z_0}{H}\right)^{+}\left(1-\frac{r_0^2}{R_0^2}\right)\frac{r-R_0}{r}\left(-\frac{1}{a^2}+\frac{1}{r_1'^2}\right)\cos\theta \tag{30}$$

3. In the region $r_1>a$ and $r_1'>a$

$$\frac{U_r}{U_{0s}}=\frac{R_0\delta^2}{2z_0}\left(\frac{z_0}{H}\right)^{+}\left(1-\frac{r_0^2}{R_0^2}\right)\frac{1}{r}\left(\frac{z-z_0}{r_1^2}-\frac{z+z_0}{r_1'^2}\right)\cos\theta$$
$$+\left(\frac{z}{H}\right)^{+}\left(1-\frac{r_0^2}{r^2}\right)\cos\theta \tag{31}$$

$$\frac{U_\theta}{U_{0s}}=-\left(\frac{z}{H}\right)^{+}\left(1+\frac{r_0^2}{r^2}\right)\sin\theta \tag{32}$$

$$\frac{U_z}{U_{0s}}=\frac{R_0\delta^2}{2z_0^2}\left(\frac{z_0}{H}\right)^{+}\left(1-\frac{r_0^2}{R_0^2}\right)^{r-R_0}\left(-\frac{1}{r_1^2}+\frac{1}{r_1'^2}\right)\cos\theta \tag{33}$$

Applying the above equations, the velocity distribution is calculated along the line which is vertical to the channel bed and passing the vortex axis in the stagnation plane. The result is shown in Fig. 16. It is recognized from this figure that the calculated values show the best agreement with measured values when k = 2, where k denotes the ratio a/z_0. Accordingly k = 2 is used hereafter, and it should be noticed that this value of k is equal with that under laminar conditions.

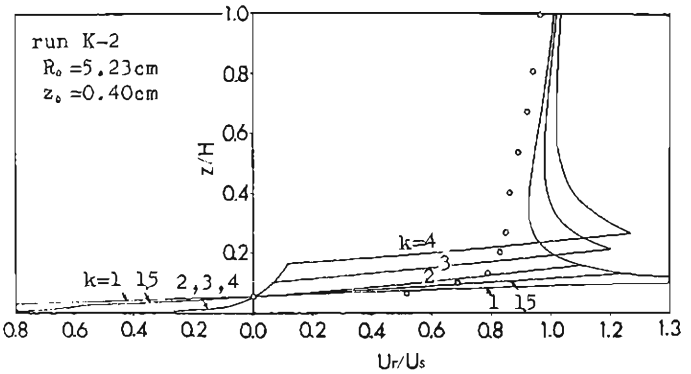

Fig. 16 Experimental verifiction of equations (25), (28) and (31) with regard to the velocity distribution on the vertical line passing the main vortex axis in the stagnation plane (run K-2)

(3) Examination of an Applicability of the Method of Analysis

The above mentioned analysis does not only sustains the primary assumptions on which the analysis of laminar flow is based, but also contains additional assumptions that turbulent fluctuations and existence of small vortices should be neglected.

As a result, the primary restrictions mentioned in 3 (2) are also imposed on the application of the above equations. For example, owing to the assumption used in composing the flow model, the vortex region of doughnut type should be under the water surface and this restriction is written as follows

$$(k+1)z_0 \leqq H \tag{34}$$

Table 3 Upper limit of r_0/H in which the analys is applicable

R_{ei}	a_3	m_3	upper limit of r_0/H
10^3	0.13	1.0	2.6
5×10^3	0.08	0.8	6.0
10^4	0.06	0.7	11.6

Substituting into this equation the equation (22) and k = 2, and using the experimental results shown in Fig. 13, the upper limit of r_0/H in which the analysis given above is applicable is obtained as shown in Table 3.

The calculated distribution of velocity at the height of $3H/4$, $H/2$, $H/4$ and $H/8$ in stagnation plane is shown in Fig. 17 compared with the measured value under the experimental conditions of run K-1. It can be seen from this figure that the calculated values show good agreement with the measured value in the neighbourhood of the vortex. On the other hand, the agreement near water suface is not so good, which is thought to be based on the reason that the vorticity around there is neglected in this analysis.

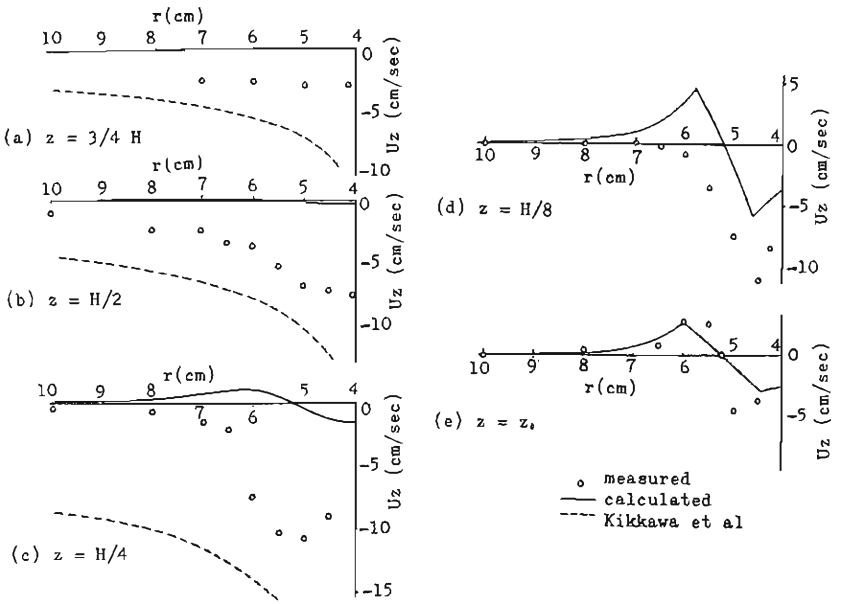

Fig. 17 Experimental verification of equations (25) ~ (33) with regard to the z component of velocity in the stagnation plane (run K-1)

In Fig. 18, vertical distribution of U_r and U_θ at $r = 5.23$ cm (position of the vortex axis) and $r = 6.5$ cm in each section of $\theta = 180°$, $210°$, $240°$ and $270°$ are shown. The agreement between calculated values and measured ones is fairly good.

6. Concluding Remarks

Detailed phenomenon of a local flow is made clear and three-dimensional distribution of velocity just upstream of a bridge pier settled on a flat bed is formulated on the basis of the experiment.

This study is characterized by the following two points; (1) Experiments are made under laminar conditions as well as turbulent conditions, by which complicated phenomenon containing vortex motion is simplified and basic hydraulic characteristics

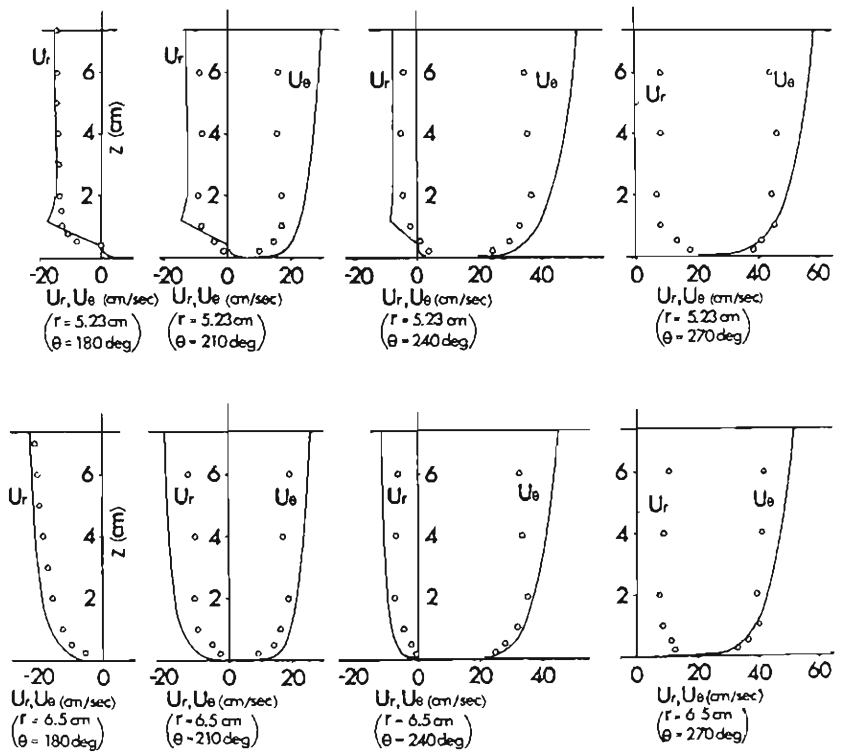

Fig. 18 Experimental verification of equations (25) ~ (33) with regard to r- and θ components of velocity (run K-1)

are made clear. (2) Measurements and analysis are made from the point of view that horseshoe vortex plays an important role on the formulation of local flows and local scours.

The main conclusions attained are: (1) There occur one or several horseshoe vortices around a bridge pier. The number and the stability of them depend on the Reynolds number, and the flow pattern in a stagnation plane under turbulent conditions is shown schematically in Fig. 9. (2) The fluid constituting these vortices is supplied from the main flow, and these vortices occur due to the concentration of vorticity which had been contained in the main flow. The process of concentration obeys the vorticity conservation law of Helmholtz. (3) Time averaged position of the main vortex axis is nearly concentric with the pier and parallel to the channel bed. It is given by equations (21) and (22) according to the above experiments. (4) Three-dimensional velocity distribution of the flow upstream of a circular pier is given by equations (11) ~ (19) for laminar conditions and by (25) ~ (33) for turbulent conditions.

Further experimental studies are scheduled on the estimating method of scour depth around bridge piers and on the method of deducing them.

Acknowledgement

The author is indebted to Dr. Yasuo Ishihara for his valuable discussions and suggestions concerning this paper.

References

1) Keutner, C. : Strömungsvorgänge an Strompfeilern von Verschiedenen Grundrissformen und Ihre Einwirkung auf die Flussohle, Die Bautechnik, Jahrgang 10, Heft 12, 1932, pp. 161-170.
2) Tison, L. J. : Érosion autour de Piles de Ponts en Rivière, Annales des Travaux Publics de Belgique (Brussels), 1940, pp. 813-868.
3) Ishihara, T. : Experimental Study of River-Bed Scour due to Bridge Piers (No. 3), Proc. JSCE, Vol. 28, No. 11, 1942, pp. 974-1007.
4) Posey, C. J. : Why Bridge Fail in Floods, Civil Engineering, Vol. 19, 1949, p. 42 and 90.
5) Laursen, E. M. and A. Toch : Scour around Bridge Piers and Abutments, Iowa Highway Research Board Bulletin, No. 4, 1956.
6) Neil, C. R. : River-Bed Scour, Technical Publication, No. 623, Canadian Good Roads Association, Ottawa, Canada, 1964.
7) Roper, A. T., V. R. Schneider and H. W. Shen : Analytical Approach to Local Scour, Proc. 12th Congress of IAHR, Vol. 3, Colorado State University, USA, 1967, pp. 151-161.
8) Shen, H. W., S. Karaki and Y. Ogawa : Time Variation of Bed Deformation Near Bridge Piers, Proc. 11th Congress of IAHR, Vol. 3, No. 3-14, Leningrad, 1965.
9) Kikkawa, H., S. Fukuoka, H. Iwama and H. Soogawa : Study on Scouring around a Bridge Pier and Its Prevention, Proc. JSCE, No. 194, 1971, pp. 83-90.
10) Nakagawa, H. and K. Suzuki : On the Flow and Local Scour around a Circular Bridge Pier, Proc. 16th Conference on Hydraulics, JSCE, 1972, pp. 31-36.
11) Squire, H. B. and K. G. Winter : The Secondary Flow in a Cascade of Airfoils in a Nonuniform Stream, Journal of the Aeronautical Science, No. 18, 1951, pp. 271-277.
12) Hawthorne, W. R. : The Secondary Flow about Strut and Airfoils, Journal of the Aeronautical Science, No. 21, 1954, pp. 588-608.
13) Lighthill, M. J. : Drift, Journal of Fluid Mechanics, Vol. 1, 1956, pp. 31-53.
14) Lamb, H. : Hydrodynamics, Cambridge, 1932.

Appendix(Notations)

x; Distance to the downstream from a axis of a circular pier or from the front side of a rectangular pier
y; Trasversal distance from the center of a channel
z; Upward distance from a channel bed
r; Radial distance from a axis of a circular pier
θ; Angle between r axis and x axis
r_0; Radius of a pier
$\bar{r}_0$; Radial distance of the boundary of displacement area from a axis of a pier
r_1; Distance from a vortex axis
r_1'; Distance from the image of a vortex axis against a channel bed
R_0; Radial distance of vortex axis from a axis of a pier
z_0; Height of vortex axis from a channel bed
U_0; Velocity distribution of approaching flow
U_{0s}; Surface velocity of approaching flow
U_x, U_y, U_z; x, y, z component of velocity
U_r, U_θ, U_z; r, θ, z component of velocity

u_r, u_θ, u_z ; r, θ, z component of velocity of a main flow
u'_r, u_θ', u'_z ; r, θ, z component of velocity of a secondary flow
a ; Radius of the vortex region which gives rise to a secondary flow
k ; $= a/z$
κ ; Circulation around a vortex region
ω_0 ; Vorticity in a vortex region $= \kappa/\pi a^2$
η ; y component of vorticity
H ; Water depth
i ; Slope of a channel bed
ν ; Kinematic viscosity
R_{ei} ; Reynolds number caculated by using water depth and friction velocity
α_1, α_2, α_3, m_1, m_2, m_3 ; Coefficient given by experiments